A Second-Order Cone Bounding Algorithm for Robust Minimum Variance Beamforming

Ngai Wong[1], Venkataramanan Balakrishnan[2], and Tung-Sang Ng[1]

[1] Department of Electrical and Electronic Engineering
The University of Hong Kong
Pokfulam Road, Hong Kong
{nwong,tsng}@eee.hku.hk
[2] School of Electrical and Computer Engineering
Purdue University
West Lafayette, IN 47907-1285, USA
ragu@ecn.purdue.edu

Abstract. We present a geometrical approach for designing robust minimum variance (RMV) beamformers against steering vector uncertainties. Conventional techniques enclose the uncertainties with a convex set; the antenna weights are then designed to minimize the maximum array output variance over this set. In contrast, we propose to cover the uncertainty by a second-order cone (SOC). The optimization problem, with optional robust interference rejection constraints, then reduces to the minimization of the array output variance over the intersection of the SOC and a hyperplane. This is cast into a standard second-order cone programming (SOCP) problem and solved efficiently. We study the computationally efficient case wherein the uncertainties are embedded in complex-plane trapezoids. The idea is then extended to arbitrary uncertainty geometries. Effectiveness of the proposed approach over other schemes and its fast convergence in signal power estimation are demonstrated with numerical examples.

1 Introduction

Antenna arrays constitute an important part in modern communication systems, serving to introduce extra degrees of freedom in beampattern synthesis, spatial filtering and/or detection of incoming signals. The design of antenna arrays when precise system parameters are available is a well-studied problem; for instance, the celebrated minimum variance (MV) beamformer, designed using Capon's method [1], has the property that the variance of the combined (i.e., weighted and summed) array output is minimized, while a unity gain is maintained in the look direction. However, in practical situations, exact models of the antenna array are unavailable. Uncertainties in the steering vector of the desired signal arise due to a multitude of reasons including array calibration errors, uncertain angle-of-arrival (AOA), amplifier imperfections and environmental inhomogeneities [2–14]. These uncertainties, when not accounted for in

the design process, can lead to severely degraded performance. For example, the performance of the MV beamformer is known to be sensitive and susceptible to mismatches in the presumed and actual steering vectors [14]. Hence we have the "robust antenna weight design problem," i.e., the design of antenna weights such that the performance can be guaranteed in spite of the presence of uncertainties.

Some approaches towards robust antenna weight design can be found in [15–21] and the references therein. For example, point and derivative constraints [15–17] imposed on the mainbeam can be used to design antenna arrays that offer tolerance against AOA mismatch, but their performance subject to other kinds of mismatches is hard to predict. The eigenspace-based beamformer in [18] is effective, although only when the signal-to-noise ratio (SNR) is high. Other methods in [17,19–21] share a similar framework wherein a certain form of weighted diagonal loading or quadratic penalty is added to the objective or cost function. The weight determination of that penalty, however, is not clear in practice. Further, these techniques assume, either explicitly or implicitly, that the uncertainty is isotropic (i.e., equally probable around the nominal steering vector) which is generally not the case. In other words, these methods or algorithms may result in overly conservative designs at the expense of other considerations such as power, complexity, and feasibility.

Recently, a number of techniques based on mathematical programming have been proposed for the robust antenna weight design of *narrowband* systems called robust MV (RMV) beamforming [2–12]. The basic idea underlying these techniques is to model the steering vector uncertainties as a convex set or part of a convex set. The antenna weights are then determined so as to minimize the maximum array output variance (or an upper bound thereof) over the steering vector uncertainty set. In [3–7], the uncertainty set is covered by a hypersphere[3] or an ellipsoid around the nominal steering vector. It can be shown that this class of beamforming techniques belongs to the diagonal loading approach, of which the amount of loading can be directly determined from the uncertainty set. The resulting optimization problem is a second-order cone programming (SOCP) problem [22, 23], which can be solved efficiently via interior point algorithms, e.g., [24–27], or by the *Lagrange multiplier* method, e.g., [4, 6]. Simulations have shown the superiority of this SOCP beamforming approach over other popular robust beamformers in adaptive arrays [3]. Nonetheless, uncertainty modeling using a worst-case hypersphere [3] is still isotropic and does not exploit the structure of the uncertainty, and may sometimes lead to impractical designs of high power requirement or even programming infeasibility. Ellipsoidal uncertainty modeling [4–7] provides tighter uncertainty modeling and generally produces more accurate results in applications such as signal power estimation [6, 7]. A different design approach is to encompass the uncertainty set by a polyhedral cone [8]. A drawback is that the use of a polyhedral cone with

[3] Here hypersphere and ellipsoid (flat ellipsoid) respectively refer to the n-dimensional counterparts of a Euclidean ball and the injective (non-injective) affine mapping of a Euclidean ball. A polyhedral cone is the set $C = \{x|Ax \leq 0\}$, i.e., C is the intersection of finitely many linear half-spaces. Specific details can be found in [2–8].

limited extreme rays (the basis rays of a cone) can again result in overly conservative constraints, while increasing the number of extreme rays will cause an exponential growth in the programming complexity and prohibit its use in larger arrays. Moreover, determination of the polyhedral cone angle in relation to the uncertainty set was not pursued further in [8].

The main contribution of this paper is that it extends the idea of a polyhedral cone to a second-order cone (SOC), and develops a constructive way, employing either a simple heuristic or a theoretically optimal SOCP approach, to obtain a tight SOC bounding the uncertainty set (also see [2]). The convexity of the optimization constraint is exploited such that the optimization process can be largely reduced from the whole uncertainty set to the intersection of the bounding SOC and a hyperplane *outside* the set. A special case of modeling steering vector uncertainties using complex-plane trapezoids is studied in detail. For practical reasons, extension of the proposed scheme to robust interference rejection is also considered. The corresponding narrowband beamforming task is formulated and efficiently solved as an SOCP problem. Numerical examples show that this *SOC RMV beamformer* exhibits tight uncertainty modeling, very low power requirement, and fast convergence in signal power estimation.

The paper is organized as follows. In Sect. 2, preliminaries in MV beamforming are reviewed. Sect. 3 proposes a generic algorithm for RMV beamforming utilizing a geometrical SOC bounding idea. Reduction of the optimization process from a convex set to the circumference of a hyperellipse is described. An application of the proposed SOC RMV beamforming algorithm is demonstrated, wherein steering vector uncertainties are embedded in complex-plane trapezoids. Simplification of the techniques and their extension to arbitrary uncertainty geometries are also discussed. Sect. 4 presents numerical examples and verifies the effectiveness and power efficiency of the proposed approach over other schemes. Finally, Sect. 5 presents the conclusion.

We close this section with a description of the notations used. The set of real numbers is denoted by $\mathbb{R}$ and the set of complex numbers by $\mathbb{C}$. $\mathbb{R}^N$ and $\mathbb{C}^N$ denote the set of real and complex vectors, respectively, with N components. The set $\mathbf{\Omega}$ is *convex* if $\mathbf{v}_1, \mathbf{v}_2 \in \mathbf{\Omega}$ implies $\rho_1 \mathbf{v}_1 + \rho_2 \mathbf{v}_2 \in \mathbf{\Omega}$ for every real $\rho_1, \rho_2 \geq 0$ that satisfy $\rho_1 + \rho_2 = 1$. A general convex optimization problem is the minimization of a linear function over a convex set $\mathbf{\Omega}$, namely,

$$\min(\mathbf{c}^* \mathbf{x}) \text{ subject to } \mathbf{x} \in \mathbf{\Omega} \tag{1}$$

where $\mathbf{c}$ and $\mathbf{x}$ are complex or real vectors, and $(\circ)^*$ denotes conjugate transpose which is equivalent to transpose, $(\circ)^T$, for real vectors. A second-order cone or SOC is a special convex set whose definition, for an "upright" SOC of dimension $2N$ and a cone angle parameter λ, is

$$\mathcal{K}_\lambda = \left\{ \begin{bmatrix} x_1 \\ \mathbf{x_2} \end{bmatrix} \;\middle|\; x_1, \lambda \in \mathbb{R}, \mathbf{x_2} \in \mathbb{R}^{2N-1}, \lambda \geq 0, x_1 \geq \lambda \|\mathbf{x_2}\| \right\} , \tag{2}$$

where $\|\circ\|$ denotes the Euclidean norm. The conceptual visualization of an SOC is shown in Fig. 1. Clearly, λ is a parameter that controls the cone angle, namely,

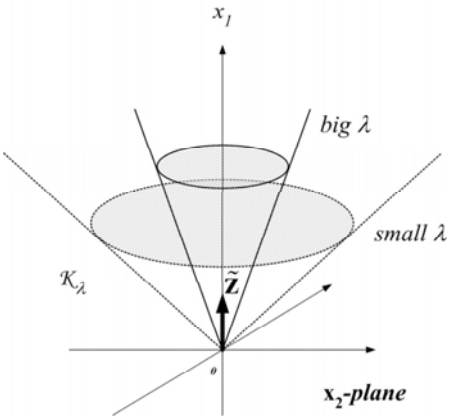

Fig. 1. An upright SOC with a variable cone angle. $\tilde{\mathbf{z}}$ is the unit vector along the symmetry axis

a large λ corresponds to a "narrow" cone and vice versa. And $\tilde{\mathbf{z}} = [\,1\,0\cdots\,0\,]^T \in \mathbb{R}^{2N}$ is the unit vector in the direction of the symmetry axis of $\mathcal{K}_\lambda$. A second-order cone programming or SOCP problem [22, 23] with real-valued variables (indicated by tildes on top, as will be followed throughout this paper) takes the form of

$$\min(\tilde{\mathbf{c}}^T\tilde{\mathbf{x}}) \text{ subject to } \tilde{\mathbf{x}} \in \mathcal{K}_\lambda \ . \tag{3}$$

It should be noted that although SOCP represents a subclass of the more general semidefinite programming (SDP) [28] (namely, the optimization of a linear function over linear matrix inequalities [29]), dedicated SOCP solvers, e.g., [25, 26], should be used [22] because of their much better worst-case complexity than general SDP solvers such as [27].

2 Background in Minimum Variance Beamforming

The output $\mathbf{x}(t) \in \mathbb{C}^N$ of an N-element antenna array is

$$\mathbf{x}(t) = \mathbf{a}(\theta)s(t) + \mathbf{A_i}\mathbf{S_i}(t) + \mathbf{n}(t) \ , \tag{4}$$

where $\mathbf{a}(\theta) \in \mathbb{C}^N$ is the steering vector of the desired *narrowband* signal $s(t)$ arriving from an angle θ, $\mathbf{A_i}$ is an $N \times L$ matrix whose lth column, $\mathbf{a}(\theta_l)$, is the steering vector of the lth interfering signal in $\mathbf{S_i}(t) = [\,s_1(t)\cdots\,s_L(t)\,]^T$, and $\mathbf{n}(t) \in \mathbb{C}^N$ is the additive noise component. The combined output of the array subject to a complex weight $\mathbf{w}$ is

$$y(t) = \mathbf{w}^*\mathbf{x}(t) \ . \tag{5}$$

The interference-plus-noise covariance matrix $\mathbf{R_{in}}$ is defined as

$$\mathbf{R_{in}} = \mathbf{E}\left((\mathbf{A_i S_i}(t) + \mathbf{n}(t))(\mathbf{A_i S_i}(t) + \mathbf{n}(t))^*\right) \ , \tag{6}$$

whereas the sample covariance matrix $\mathbf{R_x}$ is defined, and approximated by M recently received samples (called *snapshots*), as

$$\mathbf{R_x} = \mathbf{E}(\mathbf{x}\mathbf{x}^*) \approx \frac{1}{M}\sum_{p=1}^{M} \mathbf{x}(p)\mathbf{x}(p)^* \ . \tag{7}$$

One of the metrics for the performance of a beamformer is the signal-to-interference-plus-noise ratio (SINR) designated as

$$SINR = \frac{\left|\mathbf{w}^*\mathbf{a}(\theta)\right|^2 \sigma_s^2}{\mathbf{w}^*\mathbf{R_{in}}\mathbf{w}} \ , \tag{8}$$

with σ_s^2 being the signal power.

2.1 Capon Beamformer

The MV beamformer is obtained by solving

$$\min(\mathbf{w}^*\mathbf{R_x}\mathbf{w}) \text{ subject to } \mathbf{w}^*\mathbf{a}(\theta_p) = 1 \ , \tag{9}$$

where θ_p and $\mathbf{a}(\theta_p)$ are the presumed (or nominal) AOA and steering vector respectively. If this presumed steering vector matches the physical steering vector, we have the optimal solution of (9) given by the Capon's method [1]

$$\mathbf{w}_{mv} = \frac{\mathbf{R_x}^{-1}\mathbf{a}(\theta_p)}{\mathbf{a}(\theta_p)^*\mathbf{R_x}^{-1}\mathbf{a}(\theta_p)} \ . \tag{10}$$

In beampattern synthesis, it may be desirable to allow for AOA uncertainty by maintaining unity gain in a small spread of angles [4]. This is done in the MV beamforming by adding extra equality constraints. For example, defining the matrix $\mathbf{C} = [\mathbf{a}(\theta_p)\ \mathbf{a}(\theta_{p1})\ \mathbf{a}(\theta_{p2})\cdots]$ where θ_{pi}'s are angles around θ_p, and replacing the optimization constraint in (9) by

$$\mathbf{C}^*\mathbf{w} = \mathbf{d} \tag{11}$$

where $\mathbf{d}$ is a column vector of ones, the optimal weight vector is now [4, 12]

$$\mathbf{w}_{mv} = \mathbf{R_x}^{-1}\mathbf{C}(\mathbf{C}^*\mathbf{R_x}^{-1}\mathbf{C})^{-1}\mathbf{d} \ . \tag{12}$$

This formulation can also be used to introduce nulling at the interference angles if we define, with respect to (4), $\mathbf{C} = [\mathbf{a}(\theta)\ \mathbf{A_i}]$ and $\mathbf{d} = [1\ \xi_1 \cdots \xi_L]^T$ where $\xi_l \geq 0, l = 1, 2, \cdots, L$, are the desired interference gains (some small real values or zero) for signals coming from θ_l. Roughly speaking, the introduction of each equality constraint at a certain angle reduces one degree of freedom in the choice of the weight vector. Therefore, smaller arrays are more likely to yield infeasible designs when the constraints are stringent.

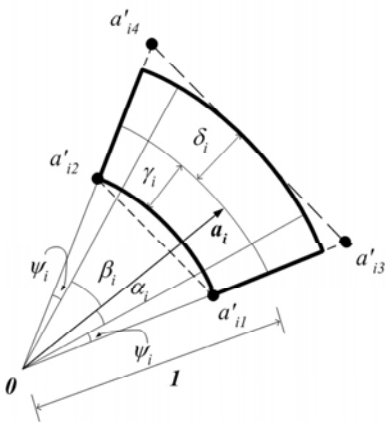

Fig. 2. Uncertainty region of a steering vector element (annulus sector in bold line) bounded by a trapezoid of vertices a'_{i1}, a'_{i2}, a'_{i3} and a'_{i4}. Here α_i, β_i, γ_i, δ_i, $\psi_i \geq \mathbf{0}$

2.2 Robustness against Signal Steering Vector Uncertainties

Let the signal steering vector be $\mathbf{a} = [\, a_1 \cdots a_N \,]^T \in \mathbb{C}^N$. Referring to Fig. 2, an element a_i of $\mathbf{a}$ may be subject to phase uncertainties, α_i, β_i, due to uncertain AOA, and phase and gain uncertainties, ψ_i, γ_i and δ_i, due to amplifier tolerance. Thus in practice a_i may assume any value inside the bolded annulus sector in Fig. 2. Let $\mathbf{\Omega} \subset \mathbb{C}^N$ be the set that contains all the possible $\mathbf{a}$ s (corresponding to all possible combinations of a_i, $i = 1, 2, \cdots, N$). An RMV beamformer [2–8] is then designed by maintaining at least a unity gain for all members in $\mathbf{\Omega}$:

$$\min(\mathbf{w}^* \mathbf{R_x} \mathbf{w}) \text{ subject to } \mathrm{Re}(\mathbf{w}^* \mathbf{a}) \geq 1, \ \forall \mathbf{a} \in \mathbf{\Omega} \tag{13}$$

where $\mathrm{Re}\,(\circ)$ and $\mathrm{Im}\,(\circ)$ (to appear later) give the real and imaginary parts of the argument.

2.3 Robustness against Interference Uncertainties

In theory, the programming solution to (13) (namely, minimizing the output power subject to signal protection) automatically achieves interference rejection. But in practice the tolerance in the amplifier implementation may render different gains and phases from the designed values. In mobile or imperfect channel scenario, drifting of the interference angle(s) may also occur between updates of weights in an adaptive array. To maintain a high SINR, as will be seen in the numerical examples, it is of value to explore robust interference rejection. Similar to the case of the nominal steering vector, uncertainties in interference rejection can be lumped as uncertainties in the interference steering vectors. Suppose $\mathbf{a}_l$ $(l = 1, 2, \cdots, L)$ is contained in the uncertainty sets $\mathbf{\Omega}_l \subset \mathbb{C}^N$, then it is desirable

that the array look direction constraint and the interference rejection constraints hold simultaneously, namely,

$$\begin{aligned} &\min(\mathbf{w}^*\mathbf{R}_\mathbf{x}\mathbf{w}) \text{ subject to} \\ &\begin{cases} \mathrm{Re}(\mathbf{w}^*\mathbf{a}) \geq 1 \ , \ \forall \mathbf{a} \in \mathbf{\Omega} \\ \|\mathbf{w}^*\mathbf{a}_l\| \leq \xi_l \ , \ \forall \mathbf{a}_l \in \mathbf{\Omega}_l \ , \ l = 1, 2, \cdots, L \ . \end{cases} \end{aligned} \tag{14}$$

The inequality settings, instead of equalities, in the interference rejection constraints lend themselves to compatibility in programming formulation as will become evident later.

2.4 Solution via Convex Optimization

One numerical approach towards the solution of (14) is based on convex optimization. The first step is to embed the uncertainty sets $\mathbf{\Omega}$ and $\mathbf{\Omega}_l$, $l = 1, 2, \cdots, L$, in convex sets (if they are not already convex); see for example, [2–9]. An example is to use the convex hulls, in the form of convex polytopes[4], of $\mathbf{\Omega}$ and $\mathbf{\Omega}_l$. Then, from convexity, it suffices to check that the look direction constraint and interference rejection constraints are satisfied on the vertices of these uncertainty convex hulls. Therefore, by choosing the enclosing convex sets appropriately, an infinite set of optimization constraints can be reduced to those on the vertices of a hull, or on the curved boundary of an arbitrary convex geometry. Nonetheless, the complexity of the hull, in terms of its number of vertices, still increases exponentially with the number of antenna element N and prohibits practical computation. In [3–8], hyperspheres, nondegenerate and degenerate (or flat) ellipsoids, and polyhedral cones are respectively used to enclose the uncertainties, and the programming problem is cast as an SOCP or a quadratic programming problem of order linearly dependent on N. It should, however, be noted that the approach based on hyperspheres does not exploit the uncertainty structure and may result in overly conservative designs with high power requirement or even render the design problem infeasible. Also, robust interference rejection is not addressed in these works. In contrast, we propose an approach that exploits the uncertainty structure and provides robustness against steering vector uncertainties regarding both the desired and interfering signals. The final beamforming problem is also an SOCP problem of size linearly dependent on N.

For convenience of computation and coding, complex quantities are often transformed into real quantities. Indicating real-valued matrices and vectors by tildes, we define

$$\begin{aligned} \tilde{\mathbf{w}} = \begin{bmatrix} \mathrm{Re}(\mathbf{w}) \\ \mathrm{Im}(\mathbf{w}) \end{bmatrix} , \ \tilde{\mathbf{a}} = \begin{bmatrix} \mathrm{Re}(\mathbf{a}) \\ \mathrm{Im}(\mathbf{a}) \end{bmatrix} , \ \tilde{\mathbf{a}}_l = \begin{bmatrix} \mathrm{Re}(\mathbf{a}_l) \\ \mathrm{Im}(\mathbf{a}_l) \end{bmatrix} , \\ \tilde{\mathbf{R}}_\mathbf{x} = \begin{bmatrix} \mathrm{Re}(\mathbf{R}_\mathbf{x}) & -\mathrm{Im}(\mathbf{R}_\mathbf{x}) \\ \mathrm{Im}(\mathbf{R}_\mathbf{x}) & \mathrm{Re}(\mathbf{R}_\mathbf{x}) \end{bmatrix} \ . \end{aligned} \tag{15}$$

[4] A polytope is a finite region of n-dimensional space enclosed by a finite number of hyperplanes. And the convex hull of a set of points is the smallest convex set that includes the points.

Starting with look direction constraint only, (13) can be equivalently written as

$$\min(\tilde{\mathbf{w}}^T \tilde{\mathbf{R}}_{\mathbf{x}} \tilde{\mathbf{w}}) \text{ subject to } \tilde{\mathbf{w}}^T \tilde{\mathbf{a}} \geq 1, \ \forall \tilde{\mathbf{a}} \in \tilde{\mathbf{\Omega}} \tag{16}$$

where $\tilde{\mathbf{\Omega}}$ is a set derived from $\mathbf{\Omega}$ by similarly stacking the real and imaginary parts of each element in $\mathbf{\Omega}$. To incorporate the interference rejection constraints in (14), we note that the magnitudes of the combined gains $\|\mathbf{w}^* \mathbf{a}_l\|$, $l = 1, 2, \cdots, L$, involve a quadratic relationship of the real and imaginary parts of $\mathbf{w}^* \mathbf{a}_l$ that describes a circle of radius ξ_l. To reduce the constraints into linear ones for SOCP formulation, two sufficient (stronger) conditions governing the real and imaginary parts are imposed, namely,

$$\begin{cases} -\frac{\xi_l}{\sqrt{2}} \leq \tilde{\mathbf{w}}^T \tilde{\mathbf{a}}_l \leq \frac{\xi_l}{\sqrt{2}} \\ -\frac{\xi_l}{\sqrt{2}} \leq \tilde{\mathbf{w}}^T \begin{bmatrix} \mathbf{0} & \mathbf{I} \\ -\mathbf{I} & \mathbf{0} \end{bmatrix} \tilde{\mathbf{a}}_l \leq \frac{\xi_l}{\sqrt{2}} \end{cases}, \forall \tilde{\mathbf{a}}_l \in \tilde{\mathbf{\Omega}}_l \tag{17}$$

for $l = 1, 2, \cdots, L$, where $\mathbf{0}$ and $\mathbf{I}$ are zero and identity matrices of compatible dimensions, and $\tilde{\mathbf{\Omega}}_l$ being analogous to $\tilde{\mathbf{\Omega}}$. It can be seen that (17) confines the real and imaginary parts of $\mathbf{w}^* \mathbf{a}_l$ to be within a square inscribed in the circle of radius ξ_l. Accordingly, (17) can be appended to the constraint list in (16) to achieve robust interference rejection. Since increasing the number of constraints may also lead to infeasibility in the design problem, robust interference rejection is more likely to be realized in larger arrays where more freedom is available.

2.5 Signal Power Estimation and Array Output Power

A main goal in many antenna array applications is to estimate the signal power σ_{s}^2 [6, 7]. In traditional beamforming, this is simply given by

$$\sigma_{\mathrm{s}}^2 \approx \mathbf{w}_{\mathrm{mv}}^* \mathbf{R}_{\mathbf{x}} \mathbf{w}_{\mathrm{mv}} \ . \tag{18}$$

A much more accurate estimate proposed in [6, 7], with the elimination of a "scaling ambiguity" by taking into account $\|\mathbf{a}(\theta)\| = \sqrt{N}$, can be shown to be

$$\sigma_{\mathrm{s}}^2 \approx \frac{1}{N} \frac{\|\mathbf{R}_{\mathbf{x}} \mathbf{w}_{\mathrm{rmv}}\|^2}{\mathbf{w}_{\mathrm{rmv}}^* \mathbf{R}_{\mathbf{x}} \mathbf{w}_{\mathrm{rmv}}} \tag{19}$$

where $\mathbf{w}_{\mathrm{rmv}}$ is the solution to the RMV beamformers in [3–7] or the present work.

Another power related issue is the array output power. A set of appropriately designed antenna weights will significantly suppress interference, therefore from (4) and (5) we have

$$y(t) = \mathbf{w}^* \mathbf{x}(t) \approx \mathbf{w}^* \mathbf{a}(\theta) s(t) + \mathbf{w}^* \mathbf{n}(t) \tag{20}$$

where $\mathbf{a}(\theta) s(t)$ is a column vector with time (phase) shifted versions of the desired signal $s(t)$ (e.g., see [7]). If we further assume that the signal is random over time

and uncorrelated with the noise (assumed to be white Gaussian), then the mean array output power is

$$E\left(y(t)y(t)^*\right) = \sigma_{\mathrm{s}}^2 \left\|\mathbf{w}\right\|^2 + \sigma_{\mathrm{n}}^2 \left\|\mathbf{w}\right\|^2 \tag{21}$$

where σ_{n}^2 is the noise power. The constraint of the Capon beamformer (namely, $\mathbf{w}^*\mathbf{a}(\theta_{\mathrm{p}}) = 1$) will put the first term on the right of (21) to σ_{s}^2 only, but in the robust formulation the more general form in (21) holds. A major implication is that if an analog beamformer is built, the power of the array output is then proportional to $\left\|\mathbf{w}\right\|^2$ (see also [9,22]). While in digital implementation, the input needs to be normalized by $\left\|\mathbf{w}\right\|^2$ to prevent overflow due to finite wordlengths. In both cases, $\left\|\mathbf{w}\right\|^2$ $(= \left\|\tilde{\mathbf{w}}\right\|^2$ in (15)) serves as a metric that should be kept as low as possible. Since $\left\|\mathbf{w}\right\|^2$ can also be interpreted as the power output of an array subject to unit-power signal and zero noise and interference, it is given a unit of *watt*.

3 An SOC Bounding Approach

As we have observed, the main drawback in directly solving (16), either standalone or with additional constraints in (17), is the exponential growth in the problem size when the number of antenna elements, N, grows. Our main contribution is an algorithm, called the SOC RMV beamforming algorithm, that reformulates the original problem so that the order of constraints grows linearly with N. In addition, the uncertainty structure and convexity in the optimization constraints are exploited, thereby leading to accurate and power-efficient beamformers. To simplify notations, we assume in the rest of this paper that $\mathbf{\Omega}$ and $\mathbf{\Omega}_l$ (and consequently $\tilde{\mathbf{\Omega}}$ and $\tilde{\mathbf{\Omega}}_l$) are some convex sets that encompass the signal and interference steering vector uncertainties $\mathbf{a}$ and $\mathbf{a}_l$ ($\tilde{\mathbf{a}}$ and $\tilde{\mathbf{a}}_l$), $l = 1, 2, \cdots, L$.

Two theorems central to our proposed algorithm, which are related to the convexity in the optimization constraints, are given here:

Theorem 1. *(Robust look direction constraint) Let* $\tilde{\mathbf{\Omega}} = Co\{\tilde{\mathbf{a}}_1, \tilde{\mathbf{a}}_2, \cdots, \tilde{\mathbf{a}}_n\}$, *where* Co *denotes the convex hull of a set, i.e., all convex combinations of its elements. Moreover, let* $\mathbf{0} \notin \tilde{\mathbf{\Omega}}$. *Let* $\mathcal{K}_\lambda$ *be any SOC with* $\tilde{\mathbf{\Omega}} \subset \mathcal{K}_\lambda$. *Suppose that* $\mathcal{H}$ *is a hyperplane separating* $\mathbf{0}$ *and* $\tilde{\mathbf{\Omega}}$. *Define the hyperellipse* $\tilde{\varepsilon}$ *by* $\tilde{\varepsilon} = \mathcal{K}_\lambda \cap \mathcal{H}$ *and let* $\partial\tilde{\varepsilon}$ *denote its boundary. Under these conditions, consider some* $\tilde{\mathbf{w}} \in \mathbb{R}^{2N}$. *If* $\tilde{\mathbf{w}}^T\tilde{\mathbf{a}} \geq 1$ *for all* $\tilde{\mathbf{a}} \in \partial\tilde{\varepsilon}$ *, then* $\tilde{\mathbf{w}}^T\tilde{\mathbf{a}} \geq 1$ *for all* $\tilde{\mathbf{a}} \in \tilde{\mathbf{\Omega}}$.

Remark 1. The implication of Theorem 1 is that the condition $\tilde{\mathbf{w}}^T\tilde{\mathbf{a}} \geq 1$ for all $\tilde{\mathbf{a}} \in \partial\tilde{\varepsilon}$ is sufficient for robust look direction constraint in (16) to hold.

Remark 2. The condition $\mathbf{0} \notin \tilde{\mathbf{\Omega}}$ automatically holds for any physically meaningful set of steering vectors.

Proof. The hyperplane $\mathcal{K}$ can be parameterized as

$$\mathcal{H} = \left\{\tilde{\mathbf{a}} \mid \tilde{\mathbf{b}}^T\tilde{\mathbf{a}} = 1\right\} \tag{22}$$

for some $\tilde{\mathbf{b}} \in \mathbb{R}^{2N}$. Since $\mathcal{H}$ separates $\mathbf{0}$ and $\tilde{\mathbf{\Omega}}$, we must have $\tilde{\mathbf{b}}^T\tilde{\mathbf{a}}_i \geq 1$, $i = 1, 2, \cdots, n$. Define $\tau_i = (\tilde{\mathbf{b}}^T\tilde{\mathbf{a}}_i)^{-1}$. Then, by the definition of $\mathcal{K}_\lambda$, we must have $\tau_i\tilde{\mathbf{a}}_i \in \mathcal{K}_\lambda$. Moreover, $\tau_i\tilde{\mathbf{b}}^T\tilde{\mathbf{a}}_i = 1$, or $\tau_i\tilde{\mathbf{a}}_i \in \mathcal{H}$. Thus $\tau_i\tilde{\mathbf{a}}_i \in \tilde{\varepsilon}$.

Now suppose that for some $\tilde{\mathbf{w}} \in \mathbb{R}^{2N}$, $\tilde{\mathbf{w}}^T\tilde{\mathbf{a}} \geq 1$ for all $\tilde{\mathbf{a}} \in \partial\tilde{\varepsilon}$. Then, as $\tilde{\varepsilon}$ is a convex set, we must have $\tilde{\mathbf{w}}^T\tilde{\mathbf{a}} \geq 1$ for all $\tilde{\mathbf{a}} \in \tilde{\varepsilon}$, and in particular, we must have

$$\tau_i\tilde{\mathbf{w}}^T\tilde{\mathbf{a}}_i \geq 1 \ , \ i = 1, 2, \cdots, n \ .$$

Consequently

$$\tilde{\mathbf{w}}^T\tilde{\mathbf{a}}_i \geq \tau_i^{-1} \geq 1 \ , \ i = 1, 2, \cdots, n \ , \tag{23}$$

concluding the proof. □

Theorem 2. *(Robust interference rejection) Let $\tilde{\mathbf{\Omega}}_l = Co\{\tilde{\mathbf{a}}_{l1}, \tilde{\mathbf{a}}_{l2}, \cdots, \tilde{\mathbf{a}}_{ln}\}$ and $\mathbf{0} \notin \tilde{\mathbf{\Omega}}_l$. Let $\mathcal{K}_\lambda$ be any SOC with $\tilde{\mathbf{\Omega}}_l \subset \mathcal{K}_\lambda$. Suppose $\mathcal{H}$ is a hyperplane such that $\mathbf{0}$ and $\tilde{\mathbf{\Omega}}_l$ lie on the same side of it, with the Euclidean distance of $\mathbf{0}$ from $\mathcal{H}$ exceeding that from any point in $\tilde{\mathbf{\Omega}}_l$ (i.e., $\tilde{\mathbf{\Omega}}_l$ is "between" $\mathbf{0}$ and $\mathcal{H}$). Define the hyperellipse $\tilde{\varepsilon}_l$ by $\tilde{\varepsilon}_l = \mathcal{K}_\lambda \cap \mathcal{H}$ and let $\partial\tilde{\varepsilon}_l$ denote its boundary. Under these conditions, consider some $\tilde{\mathbf{w}} \in \mathbb{R}^{2N}$. If $\left|\tilde{\mathbf{w}}^T\tilde{\mathbf{a}}_l\right| \leq \mu_l$ for all $\tilde{\mathbf{a}}_l \in \partial\tilde{\varepsilon}_l$, then $\left|\tilde{\mathbf{w}}^T\tilde{\mathbf{a}}_l\right| \leq \mu_l$ for all $\tilde{\mathbf{a}}_l \in \tilde{\mathbf{\Omega}}_l$.*

Remark 3. Let $\tilde{\mathbf{w}}' = \begin{bmatrix} \mathbf{0} & -\mathbf{I} \\ \mathbf{I} & \mathbf{0} \end{bmatrix} \tilde{\mathbf{w}}$ and $\mu_l = \frac{\xi_l}{\sqrt{2}}$, Theorem 2 implies that the conditions $\left|\tilde{\mathbf{w}}^T\tilde{\mathbf{a}}_l\right| \leq \frac{\xi_l}{\sqrt{2}}$ and $\left|\tilde{\mathbf{w}}'^T\tilde{\mathbf{a}}_l\right| \leq \frac{\xi_l}{\sqrt{2}}$ for all $\tilde{\mathbf{a}}_l \in \partial\tilde{\varepsilon}_l$, $l = 1, 2, \cdots, L$, are sufficient for the robust interference rejection constraints in (17) to hold.

Proof. Follows similarly to that of Theorem 1, and is therefore omitted. □

With reference to Fig. 3, the proposed SOC RMV beamforming algorithm is summarized in the following three steps:

1. Fit an SOC around the hull of $\tilde{\mathbf{\Omega}}$. If robust interference rejection is needed, also find SOCs around the hulls of $\tilde{\mathbf{\Omega}}_l$, $l = 1, 2, \cdots, L$.
2. Intersect the SOC with a hyperplane tangent to the bottom of the hull of $\tilde{\mathbf{\Omega}}$, thus forming a hyperellipse with boundary $\underline{\sigma}$ (Fig. 3(a)). In the case of robust interference rejection, hyperplanes tangent to the top of the hulls of $\tilde{\mathbf{\Omega}}_l$ are found, forming hyperellipses of boundaries $\bar{\sigma}_l$, $l = 1, 2, \cdots, L$ (Fig. 3(b)).
3. Transform (16) into an SOCP problem and optimize with respect to the stronger conditions $\tilde{\mathbf{a}} \in \underline{\sigma}$, and $\tilde{\mathbf{a}}_l \in \bar{\sigma}_l$, $l = 1, 2, \cdots, L$, in (17) for robust interference rejection.

It can be seen that the constraints in step 3 represent two sets of stronger conditions. Specifically, by Theorem 1, if $\tilde{\mathbf{w}}^T\tilde{\mathbf{a}} \geq 1$ in (16) is satisfied for all $\tilde{\mathbf{a}} \in \underline{\sigma}$, it is automatically satisfied for all $\tilde{\mathbf{a}}$ on the hyperellipse, as well as all $\tilde{\mathbf{a}} \in \tilde{\mathbf{\Omega}}$ above the hyperellipse. Similarly, if the conditions in (17) are satisfied for

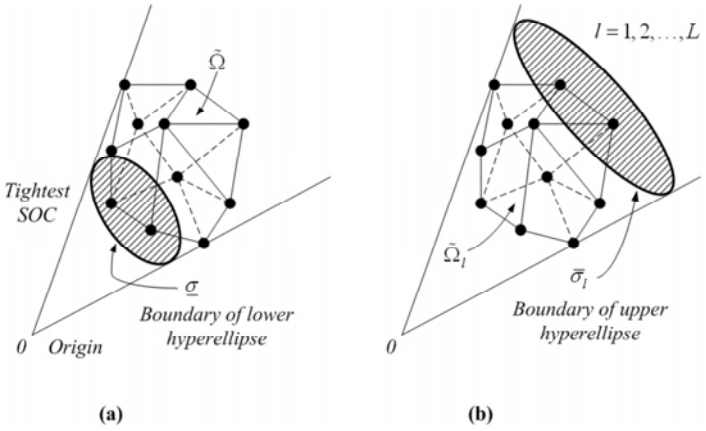

Fig. 3. A second-order cone encompassing: (a) $\tilde{\mathbf{\Omega}}$ with a lower hyperellipse; (b) $\tilde{\mathbf{\Omega}}_l$ with an upper hyperellipse

all $\tilde{\mathbf{a}}_l \in \bar{\sigma}_l$, $l = 1, 2, \cdots, L$, then by Theorem 2 they are automatically satisfied for all $\tilde{\mathbf{a}}_l$ on the hyperellipse, as well as all $\tilde{\mathbf{a}}_l \in \tilde{\mathbf{\Omega}}_l$ below the hyperellipse. The following demonstrates an application of the proposed algorithm wherein the steering vector uncertainties are modeled by complex-plane trapezoids.

3.1 Parametrizing the SOCs Bounding $\tilde{\mathbf{\Omega}}$ and $\tilde{\mathbf{\Omega}}_l$

In this step, $\mathbf{\Omega}$ and $\mathbf{\Omega}_l$, $l = 1, 2, \cdots, L$, are obtained by modeling steering vector uncertainties using complex-plane trapezoids. Subsequently $\tilde{\mathbf{\Omega}}$ and $\tilde{\mathbf{\Omega}}_l$ are derived by stacking the real and imaginary parts of each element in $\mathbf{\Omega}$ and $\mathbf{\Omega}_l$. Illustration is provided only for the location of the SOC bounding $\tilde{\mathbf{\Omega}}$, while that for the case of $\tilde{\mathbf{\Omega}}_l$ proceeds in exactly the same way. Recalling from Sect. 2 and revisiting Fig. 2, an element a_i of $\mathbf{a} = [\, a_1 \cdots a_N \,]^T$ may assume any value inside the annulus sector due to phase uncertainties, α_i, β_i, resulting from uncertain AOA, and phase and gain uncertainties, ψ_i, γ_i and δ_i, resulting from amplifier imperfections. A sensible way, which also serves as a stronger condition, is to encompass the annulus sector using a trapezoid with vertices a'_{i1}, a'_{i2}, a'_{i3}, a'_{i4} as in Fig. 2. The actual a_i may then be regarded as a convex combination of a'_{i1}, a'_{i2}, a'_{i3} and a'_{i4}, $i = 1, 2, \cdots, N$. By defining the set $\mathbf{\Omega}' \subset \mathbb{C}^N$ as the union of these vertices,

$$\mathbf{\Omega}' = \left\{ \mathbf{v}_j = [\, a'_{1k_1} \; a'_{2k_2} \cdots a'_{Nk_N} \,]^T \in \mathbb{C}^N \;\middle|\; \begin{array}{l} k_i = 1, 2, 3 \text{ or } 4 \\ i = 1, 2, \cdots, N \\ j = 1, 2, \cdots, 4^N \end{array} \right\} , \qquad (24)$$

it is clear that every point in $\mathbf{\Omega}'$ constitutes a vertex of the minimum convex hull of $\mathbf{\Omega}$. As discussed before, optimization over $\mathbf{\Omega}$ can be replaced by optimizing

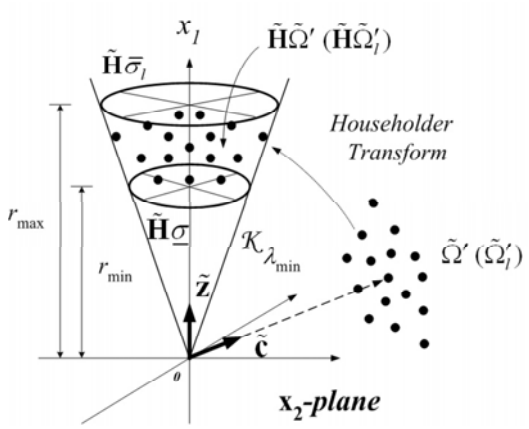

Fig. 4. Rotation of $\tilde{\mathbf{\Omega}}'$ or $\tilde{\mathbf{\Omega}}'_l$ into the bounding SOC using Householder transform

over every point in $\mathbf{\Omega}'$. Apparently, the real-valued counterpart of $\mathbf{\Omega}'$, $\tilde{\mathbf{\Omega}}' \subset \mathbb{R}^{2N}$, is formed by stacking the real and imaginary parts of every point in $\mathbf{\Omega}'$, i.e., if $\mathbf{v} \in \mathbf{\Omega}'$, then $\tilde{\mathbf{v}} \in \tilde{\mathbf{\Omega}}'$ is defined as $\tilde{\mathbf{v}} = [\mathrm{Re}(\mathbf{v}^T)\ \mathrm{Im}(\mathbf{v}^T)]^T$. Obviously, $\tilde{\mathbf{\Omega}}'$ also constitutes the vertices of the minimum convex hull of $\tilde{\mathbf{\Omega}}$. Instead of directly finding the SOC that encloses $\tilde{\mathbf{\Omega}}'$, $\tilde{\mathbf{\Omega}}'$ is first rotated, using the angle and distance preserving *Householder transform* [8], into the orientation of the upright SOC to find the SOC that just contains the rotated $\tilde{\mathbf{\Omega}}'$, denoted as $\tilde{\mathbf{H}}\tilde{\mathbf{\Omega}}'$ (or $\tilde{\mathbf{H}}\tilde{\mathbf{v}}$ for all $\tilde{\mathbf{v}} \in \tilde{\mathbf{\Omega}}'$) in Fig. 4. Defining a unit vector $\tilde{\mathbf{c}} = [\mathrm{Re}(\mathbf{c}^T)\ \mathrm{Im}(\mathbf{c}^T)]^T \in \mathbb{R}^{2N}$ in the direction of $\tilde{\mathbf{\Omega}}'$, we have

$$\tilde{\mathbf{H}} = \begin{cases} \mathbf{I} - 2\frac{(\tilde{\mathbf{c}}-\tilde{\mathbf{z}})(\tilde{\mathbf{c}}-\tilde{\mathbf{z}})^T}{(\tilde{\mathbf{c}}-\tilde{\mathbf{z}})^T(\tilde{\mathbf{c}}-\tilde{\mathbf{z}})}, & \tilde{\mathbf{c}} \neq \tilde{\mathbf{z}} \\ \mathbf{I}, & \tilde{\mathbf{c}} = \tilde{\mathbf{z}} \end{cases} \tag{25}$$

where $\|\tilde{\mathbf{c}}\| = \|\mathbf{c}\| = 1$. $\tilde{\mathbf{H}}$ is a symmetric orthogonal matrix such that $\tilde{\mathbf{H}} = \tilde{\mathbf{H}}^T = \tilde{\mathbf{H}}^{-1}$. Now the question remains as to how to choose the unit vector $\tilde{\mathbf{c}}$ for the tightest SOC that encompasses $\tilde{\mathbf{H}}\tilde{\mathbf{\Omega}}'$, denoted as $\mathcal{K}_{\lambda_{\min}}$. Two approaches are in place that offer a tradeoff between accuracy and computational load.

Optimal Method. This method finds the $\tilde{\mathbf{c}}$ that gives the tightest possible SOC. To do this we notice from (2) that an SOC, $\mathcal{K}_\lambda$, that contains a particular $\tilde{\mathbf{v}}$ must satisfy

$$\begin{aligned} \lambda &\leq \left(\left[1\ 0 \cdots 0 \right] \tilde{\mathbf{H}}\tilde{\mathbf{v}} \right) / \left\| \mathrm{diag}\left[0\ 1 \cdots 1 \right] \tilde{\mathbf{H}}\tilde{\mathbf{v}} \right\| \\ &= \left((\tilde{\mathbf{H}}\tilde{\mathbf{c}})^T \tilde{\mathbf{H}}\tilde{\mathbf{v}} \right) / \left\| \left(\mathbf{I} - \tilde{\mathbf{H}}\tilde{\mathbf{c}}(\tilde{\mathbf{H}}\tilde{\mathbf{c}})^T \right) \tilde{\mathbf{H}}\tilde{\mathbf{v}} \right\| \\ &= (\tilde{\mathbf{v}}^T\tilde{\mathbf{c}}) / \left\| \tilde{\mathbf{v}} - (\tilde{\mathbf{v}}^T\tilde{\mathbf{c}})\tilde{\mathbf{c}} \right\| \\ &= 1/\sqrt{(\|\tilde{\mathbf{v}}\|/\tilde{\mathbf{v}}^T\tilde{\mathbf{c}})^2 - 1}\ . \end{aligned} \tag{26}$$

The second line in (26) stems from the fact that $\tilde{\mathbf{H}}\tilde{\mathbf{c}} = \tilde{\mathbf{z}} = [1\,0\cdots\,0]^T$, and the third line has the geometrical interpretation that it is the projection of $\tilde{\mathbf{v}}$ onto $\tilde{\mathbf{c}}$ divided by the norm of components in $\tilde{\mathbf{v}}$ that are orthogonal to $\tilde{\mathbf{c}}$. Apparently, λ is independent of $\tilde{\mathbf{H}}$ because the cone angle is preserved by the transform. Finding the tightest SOC is equivalent to choosing a $\tilde{\mathbf{c}}$ that maximizes the minimum λ, denoted by $\lambda_{\min}$, such that $\mathcal{K}_{\lambda_{\min}}$ contains $\tilde{\mathbf{H}}\tilde{\mathbf{v}}$ for all $\tilde{\mathbf{v}} \in \tilde{\mathbf{\Omega}}'$. This statement can be restated as a programming problem in variable $\tilde{\mathbf{c}}$:

$$\max_{\|\tilde{\mathbf{c}}\|=1} \left(\min_{\tilde{\mathbf{v}}\in\tilde{\mathbf{\Omega}}'} \left(\frac{\tilde{\mathbf{v}}^T\tilde{\mathbf{c}}}{\|\tilde{\mathbf{v}}\|}\right) \right) \text{ where } \tilde{\mathbf{v}}^T\tilde{\mathbf{c}} > 0 \ , \tag{27}$$

or qualitatively, to choose a unit vector $\tilde{\mathbf{c}}$ such that the minimum projection of those unit vectors $\tilde{\mathbf{v}}/\|\tilde{\mathbf{v}}\|$ ($\tilde{\mathbf{v}} \in \tilde{\mathbf{\Omega}}'$) onto $\tilde{\mathbf{c}}$ is maximized. Clearly, $\tilde{\mathbf{c}}$ and $\tilde{\mathbf{v}}/\|\tilde{\mathbf{v}}\|$ are all on the surface of the unit sphere. Also, the projection of $\tilde{\mathbf{v}}/\|\tilde{\mathbf{v}}\|$ ($\tilde{\mathbf{v}} \in \tilde{\mathbf{\Omega}}'$) onto $\tilde{\mathbf{c}}$ can equivalently be regarded as the projection, which is a real quantity, of $\mathbf{v}/\|\mathbf{v}\|$ ($\mathbf{v} \in \mathbf{\Omega}'$) onto $\mathbf{c}$. With reference to Fig. 2 and by symmetry argument, the vector $\mathbf{c}$ that gives the tightest SOC must have each of its components lying along the symmetry axis of the corresponding trapezoid. Using $(\circ)_i$ to denote the ith component of a vector and $\arg(\circ)$ to denote the angle of a complex quantity, we have

$$\arg\left((\mathbf{c})_i\right) = \arg(a'_{i1} + a'_{i2}) \text{ where } i = 1, 2, \cdots, N \ . \tag{28}$$

Since only the projection is of interest, the number of $\mathbf{v}_j$ in (24) to be considered is largely reduced. This is because due to symmetry about $(\mathbf{c})_i$, a vector in (24) with a particular $k_i = 1$ produces the same projection as another vector with that particular $k_i = 2$, and the same holds for the case of $k_i = 3$ and $k_i = 4$. So there are effectively 2^N $\mathbf{v}_j$s ($j = 1, 2, \cdots, 2^N$) of interest whose $k_i = 1$ or 3 ($i = 1, 2, \cdots, N$). Next, to find the magnitudes of those components in $\mathbf{c}$, we define a real vector $\hat{\mathbf{c}}$ that holds the element-wise magnitudes of $\mathbf{c}$, i.e.,

$$(\hat{\mathbf{c}})_i = |(\mathbf{c})_i| \text{ where } i = 1, 2, \cdots, N \ , \tag{29}$$

and another set of real vectors $\hat{\mathbf{v}}_j$ such that

$$(\hat{\mathbf{v}}_j)_i = \left| \left(\frac{\mathbf{v}_j}{\|\mathbf{v}_j\|}\right)_i \right| \cos\left(\frac{\alpha_i + \beta_i + 2\psi_i}{2}\right) \text{ where } i = 1, 2, \cdots, N \ , \tag{30}$$

for $j = 1, 2, \cdots, 2^N$ as described earlier. The problem of maximizing the minimum projection in (27) is then equivalent to the SOCP [22, 23] problem:

$$\begin{array}{l} \max(\tau) \text{ (or } \min(-\tau)) \text{ subject to} \\ \left\{ \begin{array}{c} 0 < \tau \le \hat{\mathbf{v}}_j^T\hat{\mathbf{c}} \text{ where } j = 1, 2, \cdots, 2^N \\ \|\hat{\mathbf{c}}\| \le 1 \end{array} \right. \end{array} \tag{31}$$

for which the optimization variables are τ and $\hat{\mathbf{c}}$. The condition $\|\hat{\mathbf{c}}\| = 1$ will automatically be satisfied because the last constraint in (31) is tight for any

optimal solution. It can be seen that (31) is essentially a linear programming problem except for the last quadratic constraint. Such SOCP structure can be solved using, say, the SOCP solver in [26]. The optimal τ thus obtained constitutes an optimal solution of (27) and can be substituted back into (26) to get the maximum $\lambda_{\min}$, namely,

$$\lambda_{\min} = \frac{1}{\sqrt{\tau^{-2} - 1}} \ . \tag{32}$$

The direction vector $\mathbf{c}$ (and thus $\tilde{\mathbf{c}}$) corresponding to this tightest SOC, $\mathcal{K}_{\lambda_{\min}}$, is then obtained through combining $\hat{\mathbf{c}}$ and (28). Referring to Fig. 4, a simple and obvious choice for the hyperplane intersecting the SOC (to be used in step 2 of the algorithm) is the one that is normal to the symmetry axis of the SOC. The parameter $r_{\min}$, which specifies the height of the supporting hypercircle resulting from the intersection, is calculated from the minimum projection of $\mathbf{v}$ ($\tilde{\mathbf{v}}$) onto $\mathbf{c}$ ($\tilde{\mathbf{c}}$). This is obtained in a straightforward manner by

$$r_{\min} = \left[\mathrm{Re}([\,a'_{11}\ a'_{21}\ \cdots\ a'_{N1}\,])\ \mathrm{Im}([\,a'_{11}\ a'_{21}\ \cdots\ a'_{N1}\,])\right] \begin{bmatrix} \mathrm{Re}(\mathbf{c}) \\ \mathrm{Im}(\mathbf{c}) \end{bmatrix} \ . \tag{33}$$

The tightest SOC that contains a particular $\mathbf{\Omega}'_l$ (the interference counterpart of $\mathbf{\Omega}'$), $l = 1, 2, \cdots, L$, is found in the same way except now the height of the upper hypercircle is of interest, which is

$$r_{\max} = \left[\mathrm{Re}([\,a'_{13}\ a'_{23}\ \cdots\ a'_{N3}\,])\ \mathrm{Im}([\,a'_{13}\ a'_{23}\ \cdots\ a'_{N3}\,])\right] \begin{bmatrix} \mathrm{Re}(\mathbf{c}) \\ \mathrm{Im}(\mathbf{c}) \end{bmatrix} \tag{34}$$

where the a'_{i3}s and $\mathbf{c}$ stand for the uncertainty vectors and orientation for $\mathbf{a}_l$ and $\tilde{\mathbf{\Omega}}'_l$, respectively.

Centroid Method. A simple heuristic that largely reduces the computation of $\mathbf{c}$ from its exponential dependence (see (31)) to linear dependence on N, at a small expense of accuracy, is to approximate the optimal $\mathbf{c}$ by the normalized (unit-length) centroid of all points in $\mathbf{\Omega}'$. Defining

$$\mathbf{a}'_k = [\,a'_{1k}\ a'_{2k}\ \cdots\ a'_{Nk}\,]^T,\ k = 1, 2, 3, 4 \ , \tag{35}$$

$\mathbf{c}$ is given by

$$\mathbf{c} = \left(\sum_{k=1}^{4} \mathbf{a}'_k\right) \Big/ \left\| \sum_{k=1}^{4} \mathbf{a}'_k \right\| \ . \tag{36}$$

Using the same notational convention as in the optimal method, $\lambda_{\min}$ is obtained by finding the particular $\hat{\mathbf{v}}_j$ that decorrelates with $\hat{\mathbf{c}}$ as much as possible. This can be achieved in just $N - 1$ comparison steps: First, the components of $\mathbf{c}$ are along the symmetry axes of the uncertainty trapezoids, so the $\hat{\mathbf{v}}_j$ definition in (30) still applies. Besides, $\hat{\mathbf{c}}$ is now a predetermined quantity as given by (36).

The next step is to arrange the magnitude components of $\hat{\mathbf{c}}$ in a particular order so that they form a descending sequence; $\lambda_{\min}$ is then given by a $\hat{\mathbf{v}}_j$ whose N components are chosen to form an ascending sequence in that particular order. Since there are N such choices of $\hat{\mathbf{v}}_j$, $\lambda_{\min}$ can be determined within $N-1$ comparisons. In contrast, it generally requires $4N$ comparisons to find the radius of the smallest hypersphere (centered at the presumed steering vector) [3] bounding the annulus sector in Fig. 2. Likewise, $r_{\min}$ and $r_{\max}$ are obtained by (33) and (34) respectively. Experiments have shown that with trapezoidal uncertainty modeling, the RMV beamformers designed using this centroid method perform almost identically as those obtained by the optimal way. Therefore, in practical situations the centroid approximation of $\mathbf{c}$ should always be used when computation is of concern, especially when N is large.

3.2 Transformation of Constraints into SOC Formulation

As discussed, the robust look direction constraint in (16) can be realized under a stronger condition, namely, on the boundary $\underline{\sigma}$ of the lower hypercircle. In Fig. 4, the boundary $\underline{\sigma}$, in a rotated manner, is

$$\tilde{\mathbf{H}}\underline{\sigma} = \begin{bmatrix} r_{\min} \\ \underline{\mathbf{u}} \end{bmatrix} \subset K_{\lambda_{\min}} \text{ where } \underline{\mathbf{u}} \subset \mathbb{R}^{2N-1},\ \|\underline{\mathbf{u}}\| = \frac{r_{\min}}{\lambda_{\min}}\ . \tag{37}$$

Noting $\underline{\sigma} = \tilde{\mathbf{H}}(\tilde{\mathbf{H}}\underline{\sigma})$, the gain constraint in (16) becomes

$$\tilde{\mathbf{w}}^T(\tilde{\mathbf{H}} \begin{bmatrix} r_{\min} \\ \underline{\mathbf{u}} \end{bmatrix}) \geq 1\ . \tag{38}$$

Let $\tilde{\mathbf{H}}_1 \in \mathbb{R}^{1\times 2N}$ be the first row of $\tilde{\mathbf{H}}$, and $\tilde{\mathbf{H}}_2 \in \mathbb{R}^{(2N-1)\times 2N}$ be $\tilde{\mathbf{H}}$ without the first row, (38) can be rewritten as

$$-\underline{\mathbf{u}}^T\tilde{\mathbf{H}}_2\tilde{\mathbf{w}} \leq r_{\min}\tilde{\mathbf{H}}_1\tilde{\mathbf{w}} - 1\ . \tag{39}$$

When $\underline{u} = -(r_{\min}/\lambda_{\min})\tilde{\mathbf{H}}_2\tilde{\mathbf{w}}/\left\|\tilde{\mathbf{H}}_2\tilde{\mathbf{w}}\right\|$, the maximum of the left hand side of (39) is achieved. And the robust look direction constraint takes the form of an SOCP constraint:

$$\left\| \frac{r_{\min}}{\lambda_{\min}}\tilde{\mathbf{H}}_2\tilde{\mathbf{w}} \right\| \leq r_{\min}\tilde{\mathbf{H}}_1\tilde{\mathbf{w}} - 1\ . \tag{40}$$

By the same token, the robust interference rejection constraints in (17) can be realized under a stronger condition, namely, on the boundary $\bar{\sigma}_l$ of the upper hypercircle. In Fig. 4, the boundary $\bar{\sigma}_l$, in a rotated manner, is given by

$$\tilde{\mathbf{H}}\bar{\sigma}_l = \begin{bmatrix} r_{\max} \\ \bar{\mathbf{u}} \end{bmatrix} \subset K_{\lambda_{\min}} \text{ where } \bar{\mathbf{u}} \subset \mathbb{R}^{2N-1},\ \|\bar{\mathbf{u}}\| = \frac{r_{\max}}{\lambda_{\min}}\ . \tag{41}$$

Let $\tilde{\mathbf{H}}_{l1} \in \mathbb{R}^{1\times 2N}$ be the first row of $\tilde{\mathbf{H}}$, and $\tilde{\mathbf{H}}_{l2} \in \mathbb{R}^{(2N-1)\times 2N}$ be $\tilde{\mathbf{H}}$ without the first row, the first equation in (17) can verified to be equivalent to

$$\left\| \frac{r_{\max}}{\lambda_{\min}}\tilde{\mathbf{H}}_{l2}\tilde{\mathbf{w}} \right\| \leq \min\left(-r_{\max}\tilde{\mathbf{H}}_{l1}\tilde{\mathbf{w}},\ r_{\max}\tilde{\mathbf{H}}_{l1}\tilde{\mathbf{w}}\right) + \frac{\xi_l}{\sqrt{2}}\ . \tag{42}$$

Also, define

$$\tilde{\mathbf{J}} = \tilde{\mathbf{H}} \begin{bmatrix} \mathbf{0} & -\mathbf{I} \\ \mathbf{I} & \mathbf{0} \end{bmatrix} \ , \tag{43}$$

and let $\tilde{\mathbf{J}}_{l1} \in \mathbb{R}^{1\times 2N}$ be the first row of $\tilde{\mathbf{J}}$, and $\tilde{\mathbf{J}}_{l2} \in \mathbb{R}^{(2N-1)\times 2N}$ be $\tilde{\mathbf{J}}$ without the first row, the second equation in (17) is equivalent to

$$\left\| \frac{r_{\max}}{\lambda_{\min}} \tilde{\mathbf{J}}_{l2} \tilde{\mathbf{w}} \right\| \leq \min\left(-r_{\max} \tilde{\mathbf{J}}_{l1} \tilde{\mathbf{w}},\ r_{\max} \tilde{\mathbf{J}}_{l1} \tilde{\mathbf{w}} \right) + \frac{\xi_l}{\sqrt{2}} \ . \tag{44}$$

3.3 Beamformer Optimization Problem in SOCP Format

Finally, let $\tilde{\mathbf{R}}_{\mathbf{x}} = \tilde{\mathbf{U}}^T \tilde{\mathbf{U}}$ be the Cholesky factorization of $\tilde{\mathbf{R}}_{\mathbf{x}}$, the objective function of the SOC RMV beamforming problem in (16) can be rewritten as $\left\| \tilde{\mathbf{U}} \tilde{\mathbf{w}} \right\|^2$. As minimizing $\left\| \tilde{\mathbf{U}} \tilde{\mathbf{w}} \right\|^2$ is the same as minimizing $\left\| \tilde{\mathbf{U}} \tilde{\mathbf{w}} \right\|$, by introducing an auxiliary variable ε, (16) is cast into a standard SOCP problem of order linearly dependent on N:

$$\begin{aligned} &\min(\varepsilon) \text{ subject to} \\ &\left\| \tilde{\mathbf{U}} \tilde{\mathbf{w}} \right\| \leq \varepsilon, \ \left\| \frac{r_{\min}}{\lambda_{\min}} \tilde{\mathbf{H}}_2 \tilde{\mathbf{w}} \right\| \leq r_{\min} \tilde{\mathbf{H}}_1 \tilde{\mathbf{w}} - 1 \ . \end{aligned} \tag{45}$$

When robust interference rejection is needed, the constraints in (42) and (44) can be appended to the constraint list in (45) as:

$$\begin{cases} \left\| \frac{r_{\max}}{\lambda_{\min}} \tilde{\mathbf{H}}_{l2} \tilde{\mathbf{w}} \right\| \leq -r_{\max} \tilde{\mathbf{H}}_{l1} \tilde{\mathbf{w}} + \frac{\xi_l}{\sqrt{2}} \\ \left\| \frac{r_{\max}}{\lambda_{\min}} \tilde{\mathbf{H}}_{l2} \tilde{\mathbf{w}} \right\| \leq r_{\max} \tilde{\mathbf{H}}_{l1} \tilde{\mathbf{w}} + \frac{\xi_l}{\sqrt{2}} \\ \left\| \frac{r_{\max}}{\lambda_{\min}} \tilde{\mathbf{J}}_{l2} \tilde{\mathbf{w}} \right\| \leq -r_{\max} \tilde{\mathbf{J}}_{l1} \tilde{\mathbf{w}} + \frac{\xi_l}{\sqrt{2}} \\ \left\| \frac{r_{\max}}{\lambda_{\min}} \tilde{\mathbf{J}}_{l2} \tilde{\mathbf{w}} \right\| \leq r_{\max} \tilde{\mathbf{J}}_{l1} \tilde{\mathbf{w}} + \frac{\xi_l}{\sqrt{2}} \end{cases} \tag{46}$$

for $l = 1, 2, \cdots, L$. SOCP solvers utilizing interior-point algorithms, e.g., [25,26], can then be used to solve for the weights of this SOC RMV beamformer. The complexity of each iteration step is $O(N^3)$, and because the number of iterations is typically around ten, the complexity of this SOCP solver approach is still $O(N^3)$. Another way of solving (45), possibly with (46), is by the Lagrange multiplier method [4, 6] whose complexity is also $O(N^3)$. However, for each low-rank update of $\tilde{\mathbf{R}}_{\mathbf{x}}$, the latter approach allows update of the weight design problem with a complexity of only $O(N^2)$, while the former approach requires recomputation every time [6].

Three additional comments are in order:

1. The final SOCP problem of the proposed beamformer is of the same order as other robust schemes in [3–7] using other uncertainty bounding geometries.

However, in the SOCP problem setup, finding the hypersphere, flat ellipsoid, or the SOC (centroid approach) that enclose the uncertainty set all require $O(N)$ work. In contrast, finding the tightest SOC (optimal approach) and the minimum volume ellipsoid [4], provided SOCP and SDP solvers are used respectively, would require $O(\rho N^3)$ and $O(\rho N^4)$ work in every iteration (e.g., [22]), where ρ is proportional to the number of vertices in the uncertainty set. Consequently, the first three schemes are more practical when computational speed is of concern or array size is large.

2. If irregular, arbitrary-shape (but convex) polytopes are used to model the uncertainty set, the maximum $\lambda_{\min}$ can be obtained in the following way: First, find the minimum enclosing sphere (MES) of all points $\tilde{\mathbf{v}}/\|\tilde{\mathbf{v}}\|$ ($\tilde{\mathbf{v}} \in \tilde{\mathbf{\Omega}}'$ or $\tilde{\mathbf{\Omega}}_l'$) on the unit sphere, which can again be cast as a standard SOCP problem:

$$\begin{aligned} &\min(\text{radius}) \text{ subject to} \\ &\|\text{point}_i - \text{center}\| \leq \text{radius}, \quad \forall \text{point}_i \ , \end{aligned} \tag{47}$$

or solved using other techniques such as the Welzl's algorithm [30] in linear time. Then $\tilde{\mathbf{c}}$ is simply the unit vector pointing towards the center of this MES, while $\lambda_{\min}$, $r_{\min}$, and $r_{\max}$ are immediately inferred from the intersection of this MES and the unit sphere. The major difficulty with this approach, however, is the poor scalability due to the exponential increase in the number of hull vertices.

3. The proposed SOC RMV beamforming approach does not require the antenna array to be linear as no special restrictions are placed on the steering vectors. RMV beamforming for general non-uniform arrays with different element patterns still proceed in the same way. The proposed SOC bounding scheme also provides a deterministic and systematic way to construct the optimization constraints given the tolerance in AOA and array amplifiers. Due to the SOCP formulation of the beamforming problem, additional requirements like power restriction on the antenna weights and beampattern tuning [9] are readily incorporated. Furthermore, simple and tight uncertainty modeling with the centroid approach enables real-time setup and computation in adaptive arrays.

4 Numerical Examples

The first example studies a 5-element uniform array separated by half wavelengths. We start with a simple case of no interfering signal. Suppose a far-field narrowband signal of unit-power is impinging on the array. The signal AOA is $+20^\circ$ with an uncertainty of $\pm 2.5^\circ$. The SNR is 10 dB and the noise is white Gaussian and uncorrelated with the signal. The array amplifiers are of unity gain with an uncertainty of ± 0.05 and a phase uncertainty of $\pm 3^\circ$. The traditional non-robust Capon MV [1], and the robust hypersphere [3], full (nondegenerate) ellipsoid [4], flat (degenerate) ellipsoid [6], as well as the proposed beamformers

are designed accordingly. The hyperspherical and the full ellipsoidal uncertainty bounding schemes are designed such that the annulus sector (Fig. 2) of each steering vector component is bounded within the uncertainty set. The hypersphere radius thus calculated is 0.8287. The flat ellipsoidal bounding is designed in a way as in [6], in which a "rank-two" flat ellipsoid is formed such that the steering vectors at the two uncertain AOA extremes are within the ellipsoid. Note that a flat ellipsoid assumes certain linear combinations of uncertainty [4] and may not include all steering vector combinations as in other robust schemes. In the proposed SOC RMV scheme, the optimal and the centroid methods give almost the same SOC, parameterized by $\lambda_{\min} = 2.3783$ and $r_{\min} = 1.9922$ for the centroid approach, and $\lambda_{\min} = 2.4345$ and $r_{\min} = 1.9822$ for the optimal approach. Fig. 5 shows the performance of various beamformers against AOA mismatch. As expected, the proposed SOC RMV beamformers corresponding to the centroid and optimal methods perform virtually the same, and thus only the one from centroid method is shown. The results are based on the theoretical covariance matrix, i.e., $M \to \infty$ in (7), e.g., see [6]. Fig. 5(a) shows that the proposed and the hypersphere schemes give the best SINR robustness, with their peak SINRs being comparable to the peak value of the Capon MV beamformer. The full and flat ellipsoid schemes have lower SINR performance but it improves when the mismatch is near the extremes. Not surprisingly, the Capon MV beamformer suffers from an abrupt decrease in SINR when the actual AOA deviates from the nominal one. Fig. 5(b) shows that the flat ellipsoidal bounding method produces the tightest results (gain ≥ 1) with respect to the specified range of uncertainty, while the hypersphere bounding method results in an "over-design" due to its inherently conservative nature. The proposed and the full ellipsoid schemes are much tighter compared to the hypersphere scheme. Fig. 5(c) investigates the accuracy of the signal power estimation, with the estimate from (18) being used for the Capon MV beamformer, and (19) being employed for the other schemes. Consistent with the results in [6], the flat ellipsoid scheme produces the most accurate estimate (0 dB) over the uncertainty range, while the proposed beamformer performs similarly to the hypersphere scheme. A major drawback of the hypersphere method is the increased power metric, proportional to $\|\mathbf{w}\|^2$ (see (21)) as illustrated in Fig. 5(d), that may cause the design to be practically infeasible. In contrast, the proposed beamformer shows a value close to the optimal value of the Capon MV beamformer. The performance of other robust schemes are in between. Next, we consider the convergence rate of signal power estimation when the sample covariance matrix is used. The results are plotted against the number of snapshots (M in (7)) in Fig. 6. Under this case of no interference, the convergence rates of all robust schemes are basically the same. Fig. 6(a) shows the power estimation in the absence of AOA mismatch, while Fig. 6(b) demonstrates how AOA mismatch can deteriorate the estimation accuracy of the Capon MV beamformer.

The second example considers a 10-element uniform array separated by half wavelengths. The unit-power signal has an AOA of $+10^{\circ} \pm 2.5^{\circ}$. Four interference signals of power 6 dB lower than the signal power are coming from -70°, -30°,

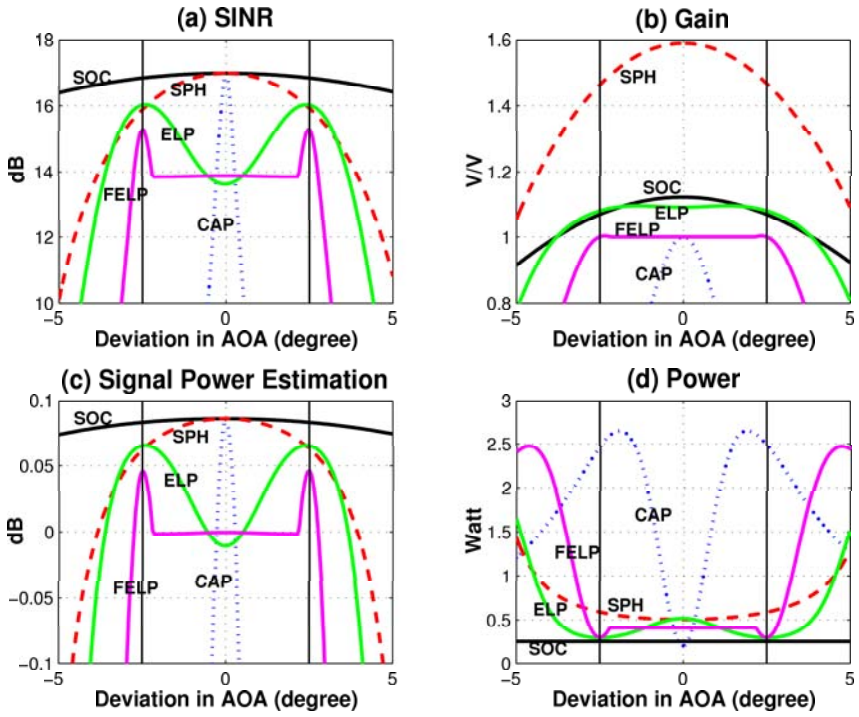

Fig. 5. (a)-(d). Performance of a 5-element array against AOA mismatch: Capon MV (CAP), hypersphere (SPH), full ellipsoid (ELP), flat ellipsoid (FELP), and the proposed (SOC) beamformers. The two vertical solid lines in each plot denote the AOA uncertainty range

$+50^{\circ}$, and $+70^{\circ}$. The noise and amplifier tolerance are the same as in the previous example. The proposed beamformer designed with the centroid and optimal approaches are again similar ($\lambda_{\min} = 0.6054$ and $r_{\min} = 2.2699$ for the centroid approach, and $\lambda_{\min} = 0.6271$ and $r_{\min} = 2.1519$ for the optimal approach) and only the results from the centroid approach are shown. The hypersphere radius in this case is 2.3847. The full ellipsoidal bounding scheme is not implemented due to its high computational complexity. Fig. 7 shows similar observations for various schemes as in Fig. 5. However, in Fig. 7(c), it can be seen that the power estimation accuracy of the flat ellipsoid scheme is strongly dependent on the actual AOA mismatch. As shown in Fig. 7(d), the variation in the power metric of different schemes is much larger due to the increased number of antennae. It can be seen that the proposed scheme maintains a near-optimal value over the whole uncertainty range. Fig. 8 further reveals that in terms of signal power estimation, the proposed scheme enjoys the fastest convergence among others.

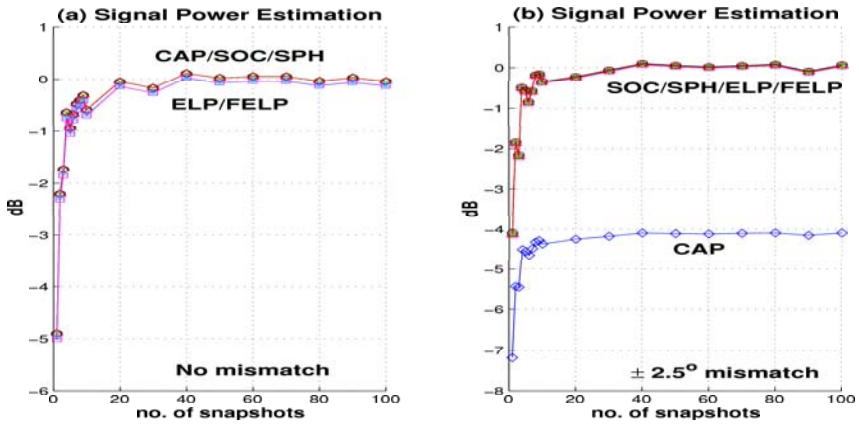

Fig. 6. Signal power estimation for a 5-element array using sample covariance matrix: (a) no AOA mismatch. (b) 2.5° AOA mismatch. Each data point is the average of 100 Monte Carlo simulations. Featured designs: Capon MV (CAP), hypersphere (SPH), full ellipsoid (ELP), flat ellipsoid (FELP), and the proposed (SOC) beamformers

In fact, our numerical experiments show that the proposed scheme consistently gives the fastest convergence.

Next, consider a case with a unit-power signal of AOA $+10^\circ \pm 1.2^\circ$. There are two unit-power interference signals from $-30^\circ \pm 0.1^\circ$ and $+50^\circ \pm 0.1^\circ$. The noise assumption is as before and the amplifier gain and phase uncertainties are ± 0.05 and $\pm 0.1^\circ$ respectively. To address the issues of amplifier and interference uncertainties, we carry out robust interference rejection as discussed in Sect. 2.3. It is required that the signal gain be at least 20 dB higher than that of the interfering signals (i.e., $\xi_1, \xi_2 < 0.1$). Fig. 9 shows 1000 random beampatterns for the Capon MV and the proposed SOC RMV beamformers (centroid approach) in which the signal AOA, interfering signal angles, and amplifier gains and phases vary randomly within their specified uncertainty ranges. The Capon MV beamformer is designed with the point nulling constraints embedded in (12), and the proposed beamformer is designed by incorporating (46) into (45). It can be seen that the worst-case performance of the Capon MV beamformer is severely degraded: the overall gain is significantly higher, admitting more noise and interference power to degrade the SINR and accuracy of signal power estimation. In contrast, the proposed scheme performs favorably against uncertainties and the beampatterns remain almost invariant. It should be noted that under these design criteria, modeling steering vector uncertainties of the desired and interfering signals using hyperspheres has rendered the SOCP problem infeasible. Table 1 gives the figures of merits for various schemes under the signal, interference, and implementation uncertainties. Specifically, the antenna weights are designed with a covariance matrix arising from a random set of data in the uncertainty set, and then the performance of the array is measured subject to

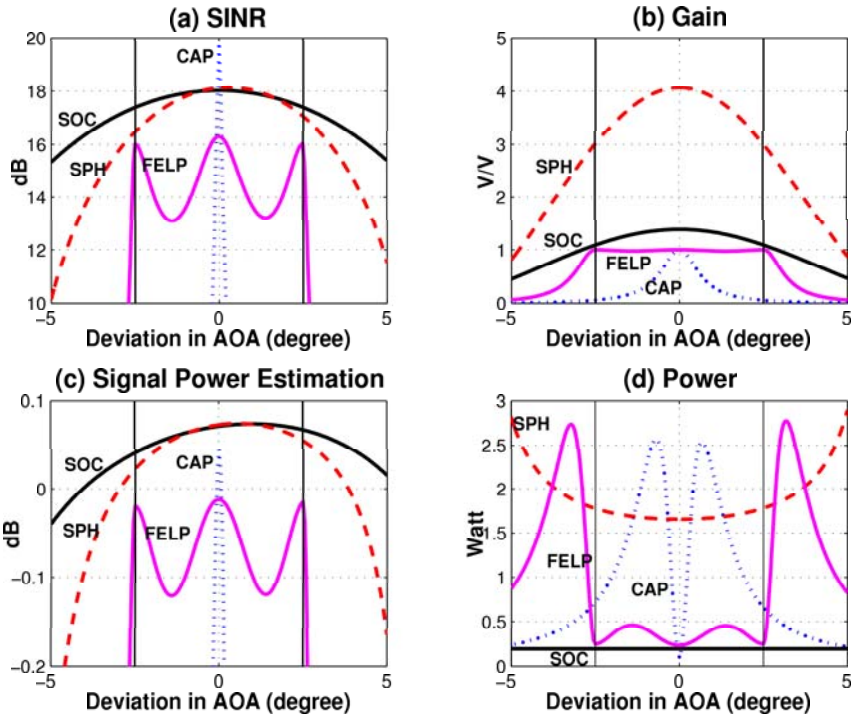

Fig. 7. Performance of a 10-element array against AOA mismatch: Capon MV (CAP), hypersphere (SPH), flat ellipsoid (FELP), and the proposed (SOC) beamformers. The two vertical solid lines in each plot denote the AOA uncertainty range

another random set of data from the uncertainty set. The results are averaged over 1000 Monte Carlo simulations. It is seen that the flat ellipsoid scheme, with its simplified uncertainty structure assumption, is most susceptible to amplifier parameter variations. While the proposed scheme with robust interference rejection delivers the highest SINR, most accurate power estimation, and low power metric. Finally, given the fact that SOC RMV beamformers resulting from the optimal method and the centroid method perform almost identically, the use of the centroid approximation in all practical cases is well justified.

5 Conclusion

This paper has presented an efficient geometrical approach for designing RMV beamformers utilizing SOC uncertainty bounding. The algorithm exploits the convexity of the optimization constraints and reduces the dimension of the optimization process from a convex hull (covering the uncertainty set) to the circumference of a hyperellipse outside the hull. Extension of this idea to robust

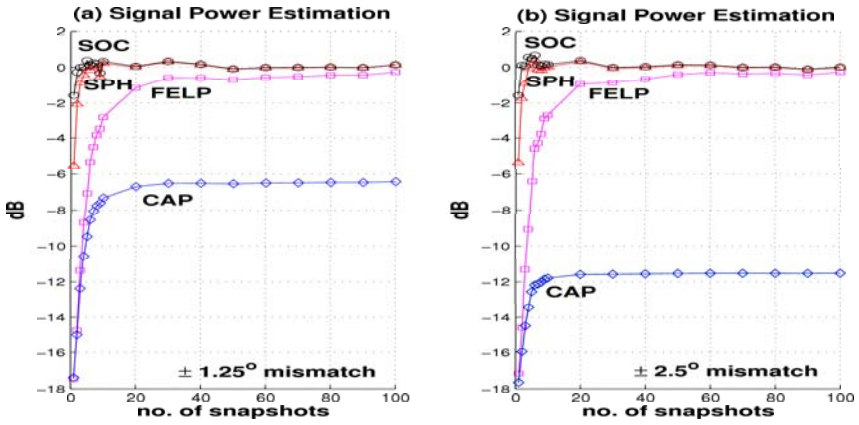

Fig. 8. Signal power estimation for a 10-element array using sample covariance matrix: (a) 1.25° AOA mismatch. (b) 2.5° AOA mismatch. Each point is obtained from the average of 100 Monte Carlo simulations. Featured designs: Capon MV (CAP), hypersphere (SPH), flat ellipsoid (FELP), and the proposed (SOC) beamformers

Table 1. Figures of merits for different schemes under signal, interference, and implementation uncertainties. 1000 Monte Carlo simulations are averaged for each entry (RIR stands for robust interference rejection)

	Power(W)	**SINR(dB)**	**Power Estimate(dB)**
Capon	1.9840	6.0621	-2.9282
Hypersphere	0.2597	18.9755	0.0768
Flat Ellipsoid	0.6754	11.7388	-0.2191
Proposed(centroid, no RIR)	0.1249	16.7159	0.1421
Proposed(optimal, no RIR)	0.1261	16.5128	0.1458
Proposed(centroid with RIR)	0.1380	19.8219	0.0515

interference rejection has been illustrated. Its application has been demonstrated through a generic example of modeling array uncertainties using complex-plane trapezoids. The beamforming task has been transformed into an SOCP problem that can be efficiently solved using either interior point algorithms or the Lagrange multiplier method. Simplification of the proposed scheme using a centroid heuristics and its extension to arbitrary uncertainty geometries have also been discussed. Numerical examples have confirmed that the proposed SOC RMV beamformer exhibits high computational efficiency, better tightness, power requirement, and convergence in signal power estimation over other schemes.

References

1. Capon, J.: Nonlinear oscillations and High-resolution frequency-wavenumber spectrum analysis. Proc. IEEE Vol. 57, No. 8 (1969) 1408-1418

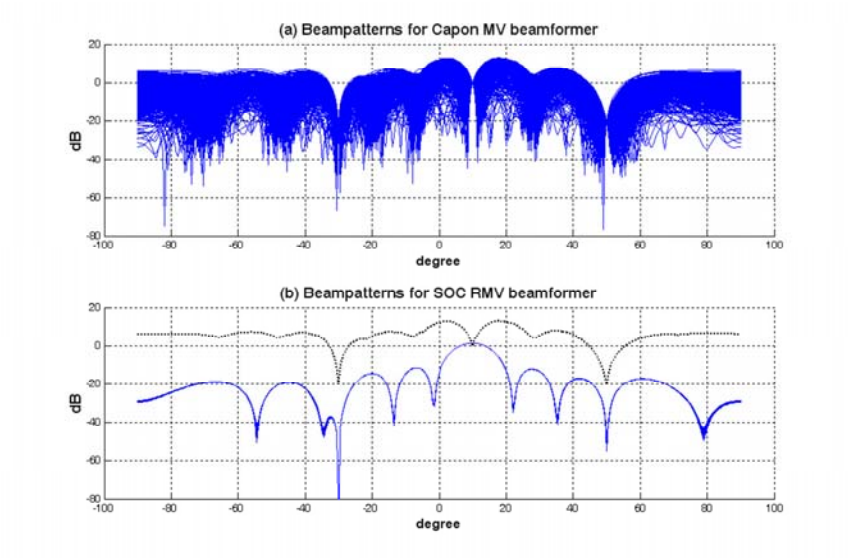

Fig. 9. (a) & (b). 1000 random beampatterns of a 10-element array featuring the Capon MV beamformer (with point interference rejection) and the proposed beamformer (with robust interference rejection), interference signals being at -30°, $+50^{\circ}$. Dotted envelope in (b) shows the maximum gain recorded in (a)

2. Wong, N., Ng, T.S., Balakrishnan, V.: A geometrical approach to robust minimum variance beamforming. Proc. IEEE Int. Conf. on Acoustics, Speech, and Signal Processing. Vol. 5 (2003) 329-332.
3. Vorobyov, S.A., Gershman, A.B., Luo, Z.Q.: Robust adaptive beamforming using worst-case performance optimization: a solution to the signal mismatch problem. IEEE Trans. Signal Processing. Vol. 51, No. 2 (2003) 313-324
4. Lorenz, R. G., Boyd, S. P.: Robust minimum variance beamforming. IEEE Trans. Signal Processing, submitted for publication (2001)
5. Lorenz, R. G., Boyd, S. P.: Robust beamforming in GPS arrays. Proc. of the Institute of Navigation, National Technical Meeting (2002)
6. Li, J., Stoica, P., Wang, Z.: On robust Capon beamforming and diagonal loading. IEEE Trans. Signal Processing. Vol. 51, No. 7 (2003) 1702-1715
7. Li, J., Stoica, P., Wang, Z.: Robust Capon beamforming. IEEE Signal Processing Letters. Vol. 10, No. 6 (2003) 172-175
8. Wu, S.Q., Zhang, J.Y.: A new robust beamforming method with antennae calibration errors. IEEE Wireless Comm. and Networking Conf. Vol. 2 (1999) 869-872
9. Wang, F., Balakrishnan, V., Zhou, P., Chen, J., Yang, R., Frank, C.: Optimal array pattern synthesis using semidefinite programming. IEEE Trans. Signal Processing. Vol. 51, No. 5 (2003) 1172-1183
10. Cantoni, A., Lin, X.G., Teo, K.L.: A new approach to the optimization of robust antenna array processors. IEEE Trans. Antennas Propagat. Vol. 41, No. 4 (1993) 403-411

11. Er, M.H., Cantoni, A.: A unified approach to the design of robust narrow-band antenna array processors. IEEE Trans. Antennas Propagat. Vol. 38, No. 1 (1990) 17-23
12. Lebret, H., Boyd, S.: Antenna array pattern synthesis via convex optimization. IEEE Trans. on Signal Processing. Vol. 45, No. 3 (1997) 526-532
13. Gershman, A.B.: Robust adaptive beamforming in sensor arrays. AEU-Int. Journal Electron. Comm. Vol. 53, No. 6 (1999) 305-314
14. Wax, M., Anu, Y.: Performance analysis of the minimum variance beamformer in the presence of steering vector errors. IEEE Trans. Signal Processing. Vol. 44, No. 4 (1996) 938-947
15. Er, M.H., Cantoni, A.: Derivative constraints for broad-band element space antenna array processors. IEEE Trans. Acoust., Speech, Signal Processing. Vol. ASSP-31 (1983) 1378-1393
16. Er, M.H., Cantoni, A.: Techniques in robust broadband beamforming. Control and Dynamic Systems: Advances in Theory and Applications, C. T. Leondes, Ed. Vol. 53, Academic Press, New York (1992) 321-386.
17. Johnson, D., Dudgeon, D.: Array Signal Processing: Concepts and Techniques. Signal Processing Series. P T R Prentice Hall, Englewood Cliffs (1993)
18. Chang, L., Yeh, C.C.: Performance of DMI and eigenspace-based beamformers. IEEE Trans. Antennas Propagat. Vol. 40 (1992) 1336-1347
19. Takao, K., Kikuma, N.: Tamed adaptive antenna array. IEEE Trans. Antennas Propagat. Vol. AP-34 (1986) 388-394
20. Cox, H, Zeskind, R.M., Owen, M.M.: Robust adaptive beamforming. IEEE Trans. Acoust., Speech, Signal Processing. Vol. ASSP-35 (1987) 1365-1376
21. Lee, C.C., Lee, J.H.: Robust adaptive array beamforming under steering vector errors. IEEE Trans. Antennas Propagat. Vol. 45, No. 1 (1997) 168-175
22. Lobo, M., Vandenberghe, L., Boyd, S., Lebret, H.: Applications of second-order cone programming. Linear Algebra and its Applications, Special Issue on Linear Algebra in Control, Signals and Image Processing. **284** (1998) 193-228
23. Alizadeh, F., Goldfarb, D.: Second-Order Cone Programming. RUTCOR RRR Report number 51-2001, Rutgers University (2001)
24. Nesterov, Yu., Nemirovskii, A.: Interior Point Polynomial Algorithms in Convex Programming. Society for Industrial and Applied Mathematics, Philadelphia (1994)
25. Lobo, M., Vandenberghe, L., Boyd, S.: SOCP: Software for second-order cone programming. *http://www.stanford.edu/~boyd/socp/*
26. Sturm, J.F.: Using SeDuMi 1.02, a MATLAB toolbox for optimization over symmetric cones. Optim. Meth. Softw. Vol. 11-12 (1999) 625-653
27. Gahinet, P., Nemirovskii, A., Laub, A., Chilali, M.: The LMI Control Toolbox. The MathWorks, Inc. (1995)
28. Vandenberghe, L., Boyd, S.: Semidefinite programming. SIAM Review. Vol. 38, No. 1 (1996) 49-95
29. Boyd, S., El Ghaoui, L., Feron, E., Balakrishnan, V.: Linear Matrix Inequalities in System and Control Theory. Vol. 15 of Studies in Applied Mathematics, SIAM, Philadelphia, PA (1994)
30. Welzl, E: Smallest enclosing disks (balls and ellipsoids). H. Maurer, editor, New Results and New Trends in Computer Science, Springer-Verlag (1991) 359-370